A 92% PCE Tri-Axis CMOS Active Receiver with LSK Modulation for Wireless Capsule Endoscopy

Alessandro Catania[1], Michele Bertozzi[1,2], Sebastiano Strangio[1], Giuseppe Iannaccone[1,3]
[1]Department of Information Engineering, University of Pisa, Pisa, Italy
[2]Clavis SRL, Pisa, Italy
[3]Quantavis SRL, Pisa, Italy
e-mail: alessandro.catania@unipi.it

***Abstract*—This work presents a tri-axis CMOS active rectifier (3AX-IC) with integrated Load-Shift Keying (LSK)-based power-state telemetry for wireless powering of capsule endoscopy systems. The proposed ASIC interfaces directly with a 3D receiver coil and integrates three identical high-efficiency rectification channels, each capable of delivering up to 225 mW, together with low-overhead telemetry modulators. The active rectifier employs a comparator-based adaptive control loop that independently regulates the switching transitions of the low-side nMOS devices, enabling near zero-voltage switching and high power conversion efficiency (PCE) across operating conditions. The LSK scheme encodes the received-power state to support transmitter-side closed-loop power control with minimal efficiency penalty. Measurement results show up to 92% PCE and robust operation under significant rotation, distance, and load variations. Combined with adaptive transmit-power control, the system maintains stable delivered power while reducing sensitivity to coupling fluctuations, making it well suited for advanced capsule endoscopy applications.**

***Index Terms*—Active Rectifier, Adaptive Power Control, Capsule Endoscopy, LSK Modulation, Wireless Power Transfer**

I. Introduction

Inductive wireless power transfer (WPT) can extend the functional lifespan of miniaturized implantable medical devices (IMDs) and, in optimal cases, eliminate the need for a battery altogether. This helps circumvent the limitations of finite energy storage, tight volume budgets, and thermal safety protocols. In practice, two fundamental challenges hinder clinical adoption. The first involves Specific Absorption Rate (SAR) regulations, which restrict the transmit field and the peak power deliverable through lossy tissue. The second stems from high sensitivity of the delivered power to relative rotation and spatial misalignment between the transmitter (Tx) and receiver (Rx) coils [1]. These challenges are acute in capsule endoscopy, which represents a critical design benchmark: the volume is restricted to a few cm^3, and the capsule experiences substantial changes in position and orientation as it moves through the gastrointestinal (GI) tract [2].

Beyond these physical constraints, the capsule subsystems dedicated to white-light imaging, sensing, and wireless data transfer impose a baseline power demand in the $100-500$ mW

This work was supported by the EC Horizon 2020 Research and Innovation Programme under GA AUTOCAPSULE 952118 and partially supported by the Italian MUR under the Forelab project of the "Dipartimenti di Eccellenza" programme.

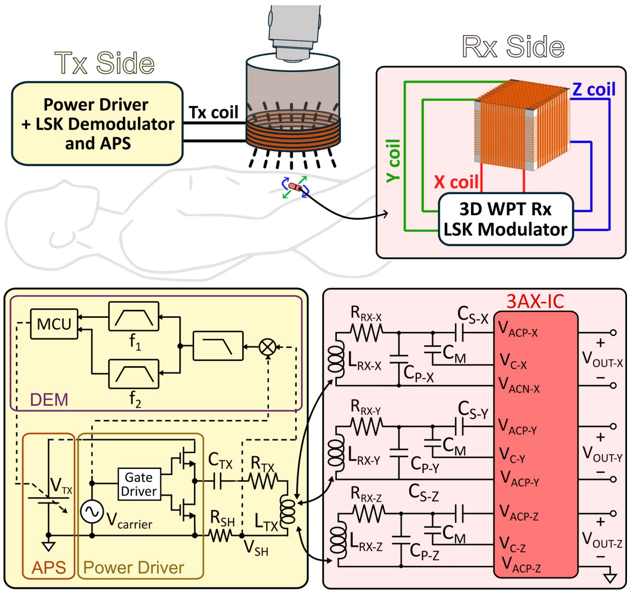

Fig. 1. Proposed inductive WPT system for wireless capsule endoscopy. The 3AX-IC is optimized for the 3D Rx coil and for the adaptive power control, guaranteeing resilience to misalignment, rotations, varying distances between Tx and Rx and varying loads.

range. Recent demonstrations of magnetically guided capsules have shown that such power levels can be delivered through tissue within SAR limits, with tight safety margins and a strong dependence on coil alignment [3]. In this work we consider a capsule that is magnetically manipulated via a robotic arm: the Tx coil is mounted at the end-effector of the arm, and the three-dimensional (3D) Rx coil (comprising three orthogonal windings) is embedded in the capsule (Figure 1). The manipulation control system maintains the capsule close to the Tx-coil axis, but significant rotation-induced and distance-induced coupling variations persist and need to be compensated.

These considerations motivate the need for WPT receivers that both mitigate orientation sensitivity and support closed-loop power regulation. Here, we present the design and the operation of 3AX-IC, a monolithic circuit fabricated in XFAB BCD-on-SOI 180 nm process that directly interfaces with the 3-axis Rx coil to reduce rotation-induced power fluctuations, and provides Load-Shift Keying (LSK) telemetry to enable closed-loop control of the transferred power, thus supporting SAR-compliant operation.

II. Circuit Architecture

Figure 2 shows the block diagram of the proposed WPT receiver architecture. The 3D Rx coil is interfaced with 3AX-IC, integrating three identical power-reception channels, one per orthogonal coil, to maximize power transfer under arbitrary orientations while maintaining a compact footprint. Each channel combines a high-efficiency active full-wave rectifier (FWR), which eliminates diode forward drops through controlled MOS conduction, with a lightweight LSK modulator [4]–[6]. The LSK encodes a three-level indication of the received power state (low, nominal, high), derived by comparing the rectified voltage against predefined thresholds and mapped onto three modulation states (no tone, f_1, f_2). This is achieved by selectively connecting an external capacitor C_M to the coil through a bootstrapped switch (M_M), inducing a detectable resonance shift at the transmitter side. The LSK modulation introduces a link efficiency penalty below 10% [3]; however, by encoding the low-power condition with no modulation, maximum efficiency is preserved when the available power is limited. A demodulator (DEM) at the Tx identifies the modulation state and closes a feedback loop that adapts the transmitted power via an adaptive power supply (APS). The modulation frequency is generated from an internal reference clock through a programmable counter (PRC). The resulting architecture enables a compact and robust WPT receiver with intrinsic resilience to rotation, distance and load variations.

Figure 3 provides further details on the active rectifier implementation. The active control loop is based on the adaptive switched-offset principle of [7], using a feedback-generated offset to calibrate the turn-on and turn-off switching events of the low-side nMOS (only one half is depicted due to the symmetry of the circuit). Unlike [7], our design replaces the hybrid delay-based gate control with two identical comparators that independently assert the turn-on and turn-off decisions. Each comparator adopts a recycling folded topology [8] with dual input pairs: the main pair compares the rectifier input voltages V_{ACP} and V_{ACN}, while an auxiliary pair injects a programmable offset. The offset is produced by a switched-capacitor integrator that samples V_{ACP} at the nMOS switching instants, and the negative-feedback loop steers the offset so that V_{ACP} is driven to approximately zero at both the turn-on and turn-off boundaries, minimizing body-diode conduction and reverse current. The operation of the two feedback paths is further clarified by the transient waveforms reported in Figure 4. To reduce power overhead, the entire loop runs from a low supply $V_{ddL} = 1.8\ V$, followed by a level shifter and buffer that drive the power nMOS gates from a higher rail $V_{ddH} = 3.3\ V$. In contrast to hybrid delay-based schemes, the proposed rectifier regulates both nMOS turn-on and turn-off through two identical offset-programmable low-power comparators, thus preserving the benefits of adaptive switched-offset calibration while avoiding delay-line sensitivity.

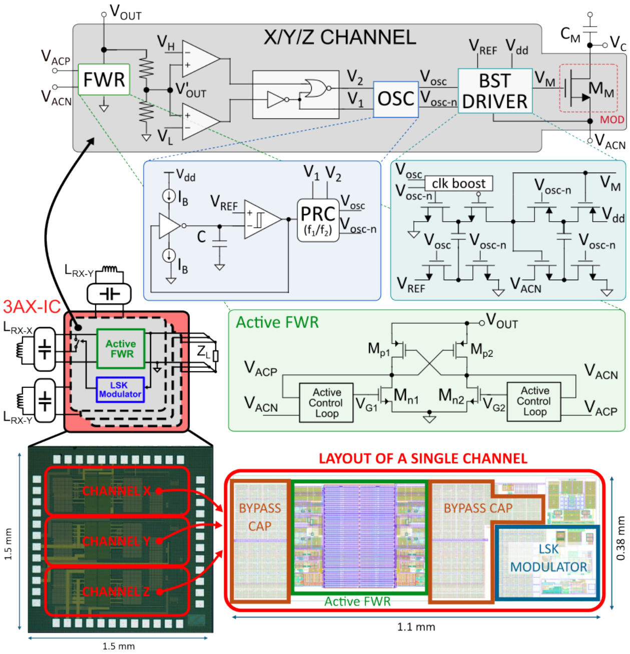

Fig. 2. 3AX-IC, fabricated in the XFAB BCD-on-SOI 180 nm process: Top: block diagram, where each channel includes an active FWR and an LSK modulator. Bottom: die micrograph and layout of a single channel.

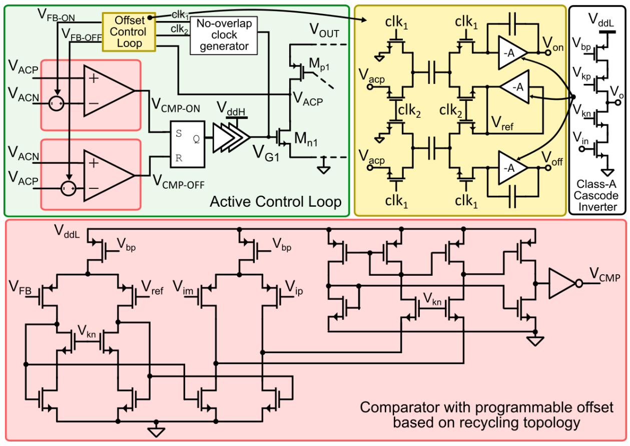

Fig. 3. Schematic view of the proposed active control loop for the active FWR.

III. Measurements and Results

The proposed 3AX-IC was experimentally characterized both in standalone conditions, by directly applying a sinusoidal input to each channel and measuring the rectified output power under different load conditions, and within the complete inductive link, to evaluate the performance of the adaptive power supply. The experimental results in Figure 5 report independent measurements for all three channels under resistive loads ranging from $60\,\Omega$ to $270\,\Omega$. For each channel, the left plot reports the Power Conversion Efficiency

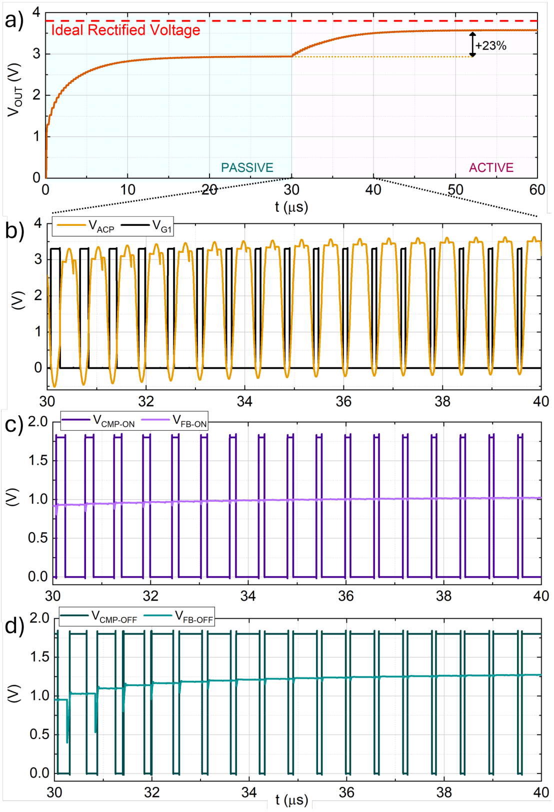

Fig. 4. Example of transient behavior of the proposed rectifier (with an input sinusoidal voltage with amplitude 3.8 V, and a load of 120 Ω). (a) Rectified output voltage $\mathrm{V_{OUT}}$ versus time, showing the transition from passive to active configuration. (b) Waveforms of $\mathrm{V_{ACP}}$ and gate control signal V_{G1} driving the nMOS transistor in the left branch. (c, d) Comparator outputs $\mathrm{V_{CMP}}$ and feedback signals $\mathrm{V_{FB}}$, for the turn-on and turn-off control, respectively. Waveforms in the right branch of the active FWR are analogous and are omitted for brevity.

$(\mathrm{PCE} = \mathrm{P_{OUT}}/\mathrm{P_{AC}})$ versus $\mathrm{P_{OUT}}$, while the corresponding right plot shows $\Delta\mathrm{PCE}$, i.e. the improvement compared to the case where the nMOS devices are kept off and thus effectively behave as passive diodes. The improvement is larger for heavier loads, while under lighter loads the net gain is limited by the fixed power consumption overhead of the active-control loop and the nMOS gate-drive buffer (total dissipation of only $0.88\,\mathrm{mW}$, including the LSK path).

Figure 6(a) shows a block diagram of the proposed APS, including the transmitter-side blocks required to close the adaptive power control loop, while Figure 6(b) demonstrates the output voltage regulation under instantaneous load variations. With the loop enabled, the output voltage is maintained within 3.3–4.2 V, with a power-update interval below 10 ms to ensure fast adaptation. Robustness to positional and rotational changes is investigated in Figure 7. The setup employed a programmable robotic arm to sweep both the distance and the orientation between the miniaturized 3D Rx coil (a cube with 1-cm sides) and a fixed Tx coil. We tested three scenarios representative of increasing resilience, namely: i) single-axis

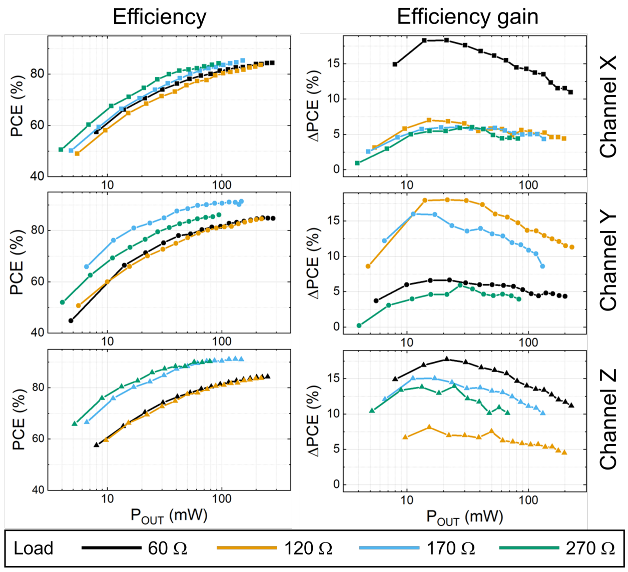

Fig. 5. Measured Power Conversion Efficiency (PCE) for different load conditions of the active FWR in the three channels (left) and PCE gain (ΔPCE) of the active FWR compared to the passive FWR (right).

operation of the 3D Rx coil with power control loop disabled, ii) simultaneous three-axis operation with power control loop disabled, and iii) three-axis operation with power control loop enabled. With single-axis operation and no power control loop, the received power exhibits large oscillations, at times collapsing to zero when the arm (and consequently the single Rx coil) passes through weak-coupling poses. When all three axes are enabled while the loop remains disabled, the received-power fluctuation is reduced, as at least one axis remains coupled throughout the experiment. Nevertheless, $\mathrm{P_{OUT}}$ is not constant due to the varying transmission distance, and the capsule experiences a fluctuating power supply margin. Finally, with tri-axial reception and adaptive power control enabled, a proportional adaptation of the transmitted power ensures that the delivered $\mathrm{P_{OUT}}$ stays within acceptable limits throughout the experiment even under aggressive rotation and distance sweeps, with dynamics compatible with capsule motion in the GI tract.

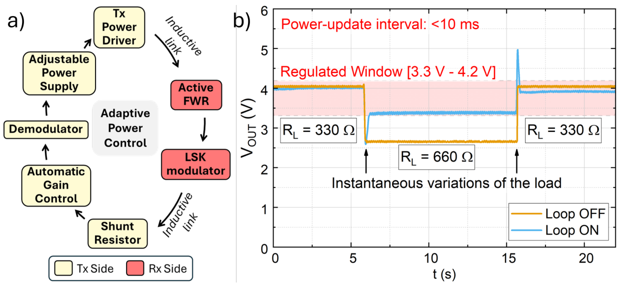

Fig. 6. Adaptive Power Control System: a) block diagram, b) comparison of the system response with/without control loop after instantaneous variations of the load.

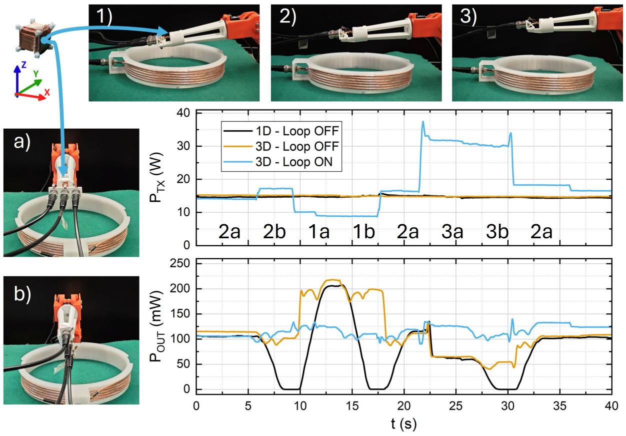

Fig. 7. Characterization of the 3D approach and the power control loop during a robotically automated set of movements of the Rx coil (with a constant load equal to 100 Ω): a) Rx Z-coil aligned with the Tx coil, b) Rx-X coil aligned with the Tx coil, and varying distances between Tx and Rx coils: 1) 4.6 cm, 2) 7.3 cm and 3) 9.5 cm.

Table I compares the proposed 3AX-IC with state-of-the-art implantable WPT receivers. Two main distinctions emerge: the proposed design integrates three receiver channels on a single die, eliminating off-chip routing and improving compactness and efficiency, and it combines high PCE with on-chip telemetry, by adopting a simple LSK scheme that encodes only the power state and enables real-time transmitter-side power regulation. The operating frequency was set to 1.7 MHz due to the limited self-resonant frequency of the fabricated tri-axial coils, rather than by intrinsic limitations of the proposed architecture. With minor retuning, the same architecture can be directly applied to ISM bands as 6.78 MHz or 13.56 MHz.

In the context of capsule endoscopy, the proposed architecture translates into clear system-level advantages. The high PCE reduces the required transmitted power, easing thermal and SAR constraints, while tri-axial reception ensures orientation diversity and robust power delivery under arbitrary poses. The closed-loop control stabilizes the output voltage, enabling reliable operation of on-board subsystems under dynamic conditions. These benefits are achieved without compromising compactness, as all three channels are integrated on a single chip. Compared to [3], which employs multi-axis reception with separate ICs and passive rectification, the proposed solution provides a more compact implementation and higher efficiency while preserving the same system-level functionality.

IV. Conclusions

The proposed 3AX-IC demonstrates that a low-overhead, compact, and robust WPT receiver for a 3D Rx coil can be effectively integrated within a single chip to support the elevated power budgets of modern capsule endoscopy systems. By combining three high-efficiency active rectifiers and LSK telemetry modulators, the ASIC maintains a stable delivered power across severe rotation and distance variations while enabling adaptive transmit-power regulation. This approach yields high PCE, strong orientation and distance resilience, and a minimal receiver footprint, providing a practical path toward reliable wireless powering of advanced implantable medical devices.

TABLE I
Comparison with state-of-the-art WPT receivers

Metric	TW	[7]	[9]	[10]	[11]	[12]
f_{res} (MHz)	**1.7**	6.78	13.56	13.56	6.78	6.78
PCE (%)	**92**	95	94.8	83.5	85.1	75.1
VCR (%)	**93.4**	97.6	94.8	83.5	85.1	-
$P_{out,max}$ (mW)	**225(1)**	125	248	1.8	2	23.7
Power control loop	**YES**	NO	NO	NO	YES	NO
CMOS (nm)	180	180	65	180	180	180
Number of channels	**3**	1	1	1	1	3
Area (mm^2)	**2.25**	2.98	1.44	2.5	2.7	4.5

(1) Per-channel.

References

[1] S. R. Khan *et al.*, "Wireless Power Transfer Techniques for Implantable Medical Devices: A Review," *Sensors*, vol. 20, no. 12, 2020.
[2] Q. Cao *et al.*, "Robotic wireless capsule endoscopy: recent advances and upcoming technologies," *Nature Communications*, vol. 15, no. 1, May 2024.
[3] A. Catania *et al.*, "In Vivo Validation of Wireless Power Transfer System for Magnetically Controlled Robotic Capsule Endoscopy," *IEEE Sensors Journal*, vol. 25, no. 24, pp. 44 729–44 739, 2025.
[4] T. Rizzo *et al.*, "A 6.78 MHz Maximum Efficiency Tracking Active Rectifier with Load Modulation Control for Wireless Power Transfer to Implantable Medical Devices," in *2022 29th IEEE International Conference on Electronics, Circuits and Systems (ICECS)*, 2022, pp. 1–4.
[5] M. Bertozzi *et al.*, "Load Modulation Feedback in Adaptive Matching Networks for Low-Coupling Wireless Power Transfer Systems," *Electronics*, vol. 12, no. 22, 2023.
[6] T. Lu and S. Du, "A 200.2-mW Wireless Power Transfer System with Hybrid SC-/RC-LSK and Triple Regulated Outputs Achieving 66.1% E2E Efficiency," in *2025 IEEE European Solid-State Electronics Research Conference (ESSERC)*, 2025, pp. 77–80.
[7] G. Namgoong *et al.*, "A 6.78 MHz, 95.0% Peak Efficiency Monolithic Two-Dimensional Calibrated Active Rectifier for Wirelessly Powered Implantable Biomedical Devices," *IEEE Transactions on Biomedical Circuits and Systems*, vol. 15, no. 3, pp. 509–521, 2021.
[8] R. S. Assaad and J. Silva-Martinez, "The Recycling Folded Cascode: A General Enhancement of the Folded Cascode Amplifier," *IEEE Journal of Solid-State Circuits*, vol. 44, no. 9, pp. 2535–2542, 2009.
[9] C. Huang *et al.*, "A Near-Optimum 13.56 MHz CMOS Active Rectifier With Circuit-Delay Real-Time Calibrations for High-Current Biomedical Implants," *IEEE Journal of Solid-State Circuits*, vol. 51, no. 8, pp. 1797–1809, 2016.
[10] M. Kim *et al.*, "A 13.56-MHz Wireless Power and Data Transfer System With Current-Modulated Energy-Reuse Back Telemetry and Energy-Adaptive Voltage Regulation," *IEEE Journal of Solid-State Circuits*, vol. 58, no. 2, pp. 400–410, 2023.
[11] D.-H. Yao *et al.*, "A 6.78-MHz Wireless Power Transfer System With Dual-Output Resonant Current-Mode Regulating Rectifier and Transmission Power Regulation," *IEEE Transactions on Circuits and Systems I: Regular Papers*, vol. 70, no. 12, pp. 4986–4998, 2023.
[12] J.-H. Kim *et al.*, "A Programming-Free Three-Dimensional Resonant Current-Mode Wireless Receiver with Real-Time Link-Adaptivity and a 0.904 cm^3 Receiver Coil for Implantable Systems," in *2025 IEEE International Solid-State Circuits Conference (ISSCC)*, vol. 68, 2025, pp. 1–3.